A large eddy simulation of the dispersion of traffic emissions by moving vehicles at an intersection

Huw Woodward[1,*], Marc Stettler[2], Dimitrios Pavlidis[3], Elsa Aristodemou[4], Helen ApSimon[1], Christopher Pain[3].

[1] *Centre for Environmental Policy, Imperial College London, SW7 2AZ, UK.*
[2] *Centre for Transport Studies, Department of Civil and Environmental Engineering, Imperial College London, SW7 2AZ, UK.*
[3] *Department of Earth Science & Engineering, Imperial College London, SW7 2AZ, UK.*
[4] *School of Engineering, London South Bank University, London, UK.*

[*] *Email: huw.woodward@imperial.ac.uk*

Abstract

Traffic induced flow within urban areas can have a significant effect on pollution dispersion, particularly for traffic emissions. Traffic movement results in increased turbulence within the street and the dispersion of pollutants by vehicles as they move through the street. In order to accurately model urban air quality and perform meaningful exposure analysis at the microscale, these effects cannot be ignored. In this paper we introduce a method to simulate traffic induced dispersion at high resolution. The computational fluid dynamics software, Fluidity, is used to model the moving vehicles through a domain consisting of an idealized intersection. A multi-fluid method is used where vehicles are represented as a second fluid which displaces the air as it moves through the domain. The vehicle model is coupled with an instantaneous emissions model which calculates the emission rate of each vehicle at each time step. A comparison is made with a second Fluidity model which simulates the traffic emissions as a line source and does not include moving vehicles. The method is used to demonstrate how the effect of moving vehicles can have a significant effect on street level concentration fields and how large vehicles such as buses can also cause acute high concentration events at the roadside which can contribute significantly to overall exposure.

Keywords: air pollution; dispersion; traffic; emissions; exposure; CFD.

1. Introduction

Commuters and residents in urban areas are often exposed to high concentrations of pollution while they travel due to their proximity to traffic emissions and the tendency to travel at peak hours. These periods of high exposure correspond to periods of higher inhalation rates for pedestrians and cyclists (de Nazelle et al., 2012). This results in a disproportionately high intake of pollutants during daily commutes which require consideration in order to fully understand the impact of poor urban air quality on health. For example, a study by de Nazelle et al. (2013) involving 36 subjects in Barcelona found that travel activities contributed to 24% of total intake of NO2, despite accounting for only 6% of time. Many studies using portable sensors have investigated the exposure of pedestrians and cyclists to particulate matter from vehicles (Berghmans et al. 2009, Int Panis et al. 2010, Kingham et al. 2013, Ragettli et al. 2013, Hankey and Marhsall 2015, Yang et al. 2015, Ham et al. 2017, Rivas et al. 2017). The concentrations experienced by pedestrians and cyclists is highly variable during any given journey, with the standard deviation of measurements often of the same order as the mean and a few acute concentration events contributing significantly to overall exposure. This is particularly true for areas with lower population density and therefore lower background PM concentration levels, for example as seen by Kingham et al. (2013). Even greater heterogeneity would be expected for the concentrations of NO2 as it is primarily emitted by vehicles and therefore concentrations near roads tend to be significantly higher than the background. Higher inhalation rates for cyclists make these peak concentration events more significant. For example, Int Panis et al. (2010) estimate a correction of 4.3 to account for the increased inhalation rate of cyclists relative to pedestrians based on field measurements for commuter cyclists. In addition, deeper inhalation during cycling leads to higher deposition of ultrafine particles in the lungs (Daigle et al., 2003). The highly variable nature of pollution concentrations within the urban environment is due to many factors including weather conditions, traffic flow rates, proximity to passing vehicles, vehicle type, isolated high pollution sources including highly polluting vehicles. The use of on-board measurement systems (Irwin et al. 2018) and portable emission measurement systems (PEMS) (O'Driscoll et al. 2016) have shown that vehicle emissions are dominated by high emission peaks during vehicle acceleration or gear changes, further contributing to the heterogeneity of concentrations within urban streets. In order to accurately evaluate the health impact of pollutants inhaled within urban areas beyond measurement field studies, the occurrence of these acute concentration events must be modelled.

It is known that traffic induced flow contributes significantly to pollution dispersion in urban areas, particularly at low wind speeds (Qin 1993). This was demonstrated in an experiment undertaken as part of the DAPPLE project (Arnold et al. 2004) in which an inert tracer was released in a street in London, concentrations of which were detected at upwind locations. It was hypothesized that these upwind concentrations were due to the entrainment of the tracer by vehicles moving upwind. While there are many modelling studies focused on understanding the dispersion of tailpipe emissions within the near-wake region of moving vehicles (e.g. Baker 2001, Dong and Chan 2006, Carpentieri et al. 2010, 2012, Tientcheu-Nsiewe et al. 2016), efforts to numerically simulate traffic induced dispersion within urban scenarios have so far been limited in number. Solazzo et al. (2007) simulated the effect of moving vehicles on air flow using moving canyon walls relative to stationary blocks representing vehicles. An averaged parameterization of the impact of traffic induced turbulence on dispersion was derived by Di Sabatino et al. (2003) and Kastner-Klein et al. (2003). This parametrization was used within a Reynolds averaged Computational Fluid Mechanics (CFD) simulation by Thaker and Gokhale (2016), however this approach does not resolve the temporal variation in concentrations and magnitude of high concentration peaks seen in field study measurements. Other Reynolds averaged simulations using a moving mesh were undertaken by Kim et al. (2016) and Dong et al. (2017). A Large Eddy Simulation (LES) approach was used by Zhang et al. (2017), where each vehicle's drag force was applied to the air using a momentum source term. Relatively simple setups in a wind tunnel with a limited number of vehicles (Pearce & Baker 1997, Ahmad et al. 2002, Kastner-Klein et al. 2001, Kastner-Klein et al. 2003) have proven to be informative, however a method for simulating complex traffic flows has yet to appear. In this paper, we investigate the combined effect of moving vehicles and time-dependent emissions at the rear of the vehicles on emission dispersion.

In order to realistically model traffic induced dispersion, it is important to use a realistic emissions model for the vehicles. It is well known that the emissions of petrol and diesel vehicles within an urban environment are highly variable, with high emission peaks occurring during high engine loads (O'Driscoll et al. 2016, Irwin et al. 2018), for example when a vehicle accelerates from standstill. The emissions model COPERT (Computer Program to Calculate Emissions from Road Transport), which is widely used across Europe, estimates the average emission factors as functions of a vehicle speed only, with the average speed along a road often used. While the model attempts to account for the higher emission rates expected at lower average speeds due to increased stopping and starting, the spatial and temporal variability is lost. Furthermore, COPERT has limitations at low vehicle speeds (<10kmph) (O'Driscoll et al.

2016), which causes further problems for urban modelling where average vehicle speeds can often be low, particularly during peak hours and near junctions.

Here, a Large Eddy Simulation (LES), computational fluid dynamics method is used to simulate the air flow and dispersion of traffic emissions due to traffic movement within an urban scenario. The open source CFD code Fluidity (http://fluidityproject.github.io/) is used to model the air flow at a crossroads consisting of four lanes of traffic for a period of low wind speed. A low wind speed case is chosen such that traffic-induced turbulence dominates as wind driven turbulence is very low within the street canyons. Fluidity's traffic-induced dispersion model is coupled with an instantaneous emissions model, where each vehicle's NOx emission is calculated as a function of the vehicle's velocity and acceleration. By considering the acceleration in addition to the velocity, a more realistic emissions model is obtained which attempts to account for the emission peaks at high engine loads. In order to provide the Fluidity traffic model and the emissions model with the required vehicle dynamics, the traffic simulation software PTV Vissim (PTV Group) is used to simulate the traffic along the crossroads geometry. The method is capable of simulating the effect of moving traffic on pollution dispersion within the street at high temporal and spatial resolution. We demonstrate the potential of the method by simulating the dispersion at the crossroads, formed by the intersection of two street canyons. Two cases are compared, one with the coupled traffic-emissions model, and one without traffic movement where the emissions are modelled as a constant line source. The impact of moving vehicles on the dispersion of emissions is investigated in addition to the effect of vehicles on the occurrence of acute high concentration events at the roadside. This work was carried out as part of the MAGIC project (http://www.magic-air.uk/).

Section 2 describes the methodology implemented, including the Fluidity traffic model, the traffic simulation (PTV Vissim) and emissions model. Section 3 describes the setup of the simulations, whilst the comparison of the two crossroads simulations is given in Section 4, along with an analysis of the effect of traffic on dispersion. A discussion of the methodology is given in Section 5 and conclusions in Section 6.

2. Methodology

The method used in this paper comprises of three parts. The first involves the computational fluid dynamics (CFD) software, Fluidity, used to simulate the airflow within the domain. Section 2.1 provides the details of the CFD methods used here. The second part described in Section 2.2 is the traffic simulation using PTV Vissim (PTV Group), which provides Fluidity with the required vehicle dynamics. The final part is the emissions model, described in Section 2.3, which is used by Fluidity to calculate the emissions of each vehicle at any given time.

2.1. Urban airflow model

Fluidity is an open-source software, developed at Imperial College London. Fluidity is a general purpose, finite-element CFD software, within which a Large Eddy Simulation (LES) methodology is implemented with an anisotropic adaptive mesh. Using the LES method, Fluidity resolves the turbulent features of the flow larger than a specified filter length by solving the filtered Navier-Stokes equations, while smaller scale eddies are modelled as additional viscosity based on a Smagorinsky-type model. Its adaptive mesh capability allows Fluidity to automatically adapt the mesh to regions of high gradients, such as evolving eddy patterns, while using a coarser mesh at more stable regions. The level of refinement is controlled by a desired interpolation error for each field, entered by the user, in addition to the chosen minimum and maximum edge lengths. The adaptive mesh technique is described in detail in (Pain et al., 2001). A variation of the Smagorinsky model, developed by (Bentham, 2003), is used to model the subgrid scale eddy viscosity. The second order scheme used here allows for anisotropic eddy viscosity where the filter length depends on the local element size, which is particularly suited for an unstructured, adaptive mesh.

Fluidity has an inbuilt traffic module capable of simulating the effect of individual vehicles on the airflow as they move through the domain. The traffic model treats the vehicles as a second fluid in a multi-fluid problem. Each vehicle is modelled as a second highly viscous fluid (essentially a solid), which displace the air around them as they flow through the domain. The problem is solved as a multi-fluid problem, however the vehicle dynamics are provided as an input and therefore the momentum equation for the vehicle “fluid” does not need to be solved. The continuity equation for this multi-fluid, incompressible flow is given by:

$$\frac{\partial}{\partial t}(\alpha_k \rho_k) + \nabla(\alpha_k \rho_k U_k) = 0, \qquad \text{for} \quad k = s, f.$$

Here s and f denote the fluid phase and stand for solid and fluid, respectively. α_k is the volume fraction of fluid k, where we have $\alpha_s + \alpha_k = 1$. ρ_k and U_k are the density and velocity of fluid k. For an incompressible problem the momentum equation for the air is given by:

$$\alpha_f \rho_f \left(\frac{\partial U_f}{\partial t} + \left(U_f - U_G\right) \cdot \nabla U_f \right) = -\alpha_f \nabla p + \nabla \cdot \left(\mu \nabla \cdot U_f + \tau_f\right) + \sigma_d \left(U_s - U_f\right),$$

where U_G is the finite element grid velocity due to the adaptive mesh, $U_s = f(\bar{x}, t)$ is the known velocity of the solid phase, p is the fluid pressure and τ_f is the unresolved turbulent stress tensor. σ_d is an absorption coefficient defined as $\sigma_d = \alpha_s \rho_f \beta / \tau_\sigma$, where $\beta \geq 1$ is a weighting factor (β is set to 1 in these simulations) and $\tau_\sigma = 1/\Delta t$ is used to relax the fluid velocity to the solid velocity in timestep Δt. The fluid equations were discretized using a continuous Galerkin discretization. The Crank-Nicholson scheme was used to discretize in time with an adaptive time step dependent on the user defined Courant number.

The last term on the right-hand side consists of both a momentum source and a sink which together apply the force of the vehicle fluid on the air. Where the vehicle velocity is greater than the fluid velocity, $U_s > U_f$, this term is positive and is therefore equivalent to a momentum source displacing the air around the solid. Where the vehicle velocity is less than the fluid velocity, $U_s < U_f$, this term is negative and therefore equivalent to an absorption term, decelerating the fluid velocity as it impacts the vehicle. It has been shown that with sufficient mesh refinement this method can be used to accurately model problems with complex solid geometries (Garcia et al, 2011).

The vehicle emissions are modelled as a passive tracer with the following advection-diffusion equation used to model its dispersion:

$$\frac{\partial c}{\partial t} + U_f \cdot \nabla c = \nabla \cdot (\kappa \nabla c) + F,$$

where c is the tracer concentration, κ is the diffusivity tensor and F is a source term. This equation is discretized using a second-order coupled finite element/control volume method.

2.2. Traffic micro-simulation

The Fluidity traffic model requires the vehicle dynamics as an input. Specifically, Fluidity requires the length, coordinates, velocity, acceleration and vehicle type at each timestep for each vehicle. For the crossroads simulation presented here this information was obtained by running a traffic simulation using the software PTV Vissim (PTV Group). PTV Vissim is primarily used for traffic management purposes and is able to simulate the movement of vehicles through a predefined geometry in order to assess traffic management decisions. The model includes a car following model, gap acceptance model and traffic regulations at intersections to provide a reasonable simulation of real-life driving behavior. The default PTV Vissim version 10 driving model was used here. The required data for each vehicle was output at 0.5 second intervals. Linear interpolation is used to obtain values at any time. The vehicle type determined the dimensions of the vehicle in addition to the emissions model to be used. The coordinates provided are only the x and y coordinates, as PTV Vissim is a two-dimensional model. A perfectly flat surface was assumed for the floor of the geometries used for the simulations in this paper.

2.3. Vehicle emissions model

The NOx emissions of each vehicle were calculated at each time step of the CFD simulation. The emissions models for diesel cars and buses developed by Panis et al. (2006) were used. The emissions calculated for each vehicle at each simulation time step are modelled as a release of a passive tracer at the rear of the vehicle. The higher temperature of the exhaust and its velocity are not considered within the model. While these are expected to affect the near-wake dispersion, they are less significant within the far-wake. The models are in the form of bivariate quadratic equations which are functions of the vehicle velocity, v_n, and acceleration, a_n, where n denotes the vehicle number:

$$E_n(t) = \max[0, f_1 + f_2 v_n(t) + f_3 v_n(t)^2 + f_4 a_n(t) + f_5 a_n(t)^2 + f_6 v_n(t) a_n(t)].$$

Here $f_1, \dots, f_6$ are coefficients derived from the measurement data using a non-linear multiple regression, where a different set of coefficients are derived for the diesel cars and the diesel buses. These coefficients are given in Table 1.

Table 1: Emission functions for diesel car and bus

Vehicle Type	f_1	f_2	f_3	f_4	f_5	f_6
Diesel car ($a \geq -0.5 m/s^2$)	2.41e−03	−4.11e−04	6.73e−05	−3.07e−03	2.14e−03	1.50e−03
Diesel car ($a < -0.5 m/s^2$)	1.68e−03	-6.62e−05	9.00e−06	2.50e−04	2.91e−04	1.20e−04
Bus	2.36e−02	6.51e−03	-1.70e−04	2.17e−02	8.94e−03	7.57e−03

These models were empirically derived from emission measurements for five diesel cars and six diesel buses taken during real urban traffic situations. These vehicles comply with different emission standards. The five diesel cars consist of two Euro 1, one Euro 2 and two Euro 3 type vehicles, while the six buses consist of two Euro 1 and four Euro 2 type vehicles, where Euro 1, 2 and 3 are vehicle emission standards defined by EU directives (91/441/EEC, 94/12/EC, 98/69/EC). These emission standards no longer represent the majority of the fleet in Europe, new vehicles are now required to comply with Euro 6 standards. However, the instantaneous emissions model derived from these measurements still provide emission peaks for periods of high engine loads as is also seen for newer engines (O'Driscoll et al., 2016). It is therefore expected that this instantaneous model can still provide a reasonable estimate of the expected variation in emissions with vehicle velocity and acceleration. While the magnitude of the total NOx emitted will be an overestimate, the total emissions can be scaled to match those expected from vehicles which comply with more recent standards. Within the context of this paper, we are not concerned with absolute values. Rather, it is our intention to demonstrate both the importance of accounting for these highly variable emissions and the potential of this method for investigating their impact on local air quality. Further work is required to derive emission models that are representative of the current fleet.

3. Model setup

In order to capture the vehicle shapes as accurately as possible, Fluidity refines the mesh at the interface between the vehicles and the air. These small mesh elements combined with the often high velocities of the vehicles lead to smaller time steps than would otherwise be the case since the maximum in-canyon velocities are likely to be lower in the absence of traffic. These small simulation time steps combined with the relatively long simulation time required to model realistic traffic scenarios currently limits the applicability of the method. Further work is required in order to investigate methods for reducing simulation run times.

3.1. Computational domain

In order to reduce the run time, a coarse mesh was used relative to the size of the vehicles. A full size geometry was used, where the vehicle size was 4.4 m x 1.5 m x 1.5 m for cars and 11.5 m x 2.55 m x 4.4 m for buses. A minimum element edge length of 0.5 m was used which sets the lower limit of the element edge length used by the adaptive mesh. Each vehicle is modelled as a rectangular block. A single vehicle simulation was used to assess the performance of the model at this resolution and the suitability of the rectangular block geometry for the vehicles; the results of the simulation are provided in Appendix A. It is shown that at this resolution the detailed flow dynamics around the vehicles is not captured, particularly in the near-wake region. However, a better approximation of the far-wake is achieved and a reasonable approximation of the overall effect of the vehicle on the flow is seen. An adaptive time step was used for the simulation, the magnitude of which is limited by setting the Courant number, which we set to equal 5. The performance of the model with this Courant number was compared against the wind tunnel setup of Di Sabatino et al. (2003), as discussed in Appendix B. The impact of the vehicles on the prevailing wind flow was in reasonable agreement for the traffic model and the wind tunnel. Similarly, the turbulent velocities were also in reasonable agreement.

The crossroads traffic simulation used here is shown in Figure 1. The model was configured such that the traffic flow rate from entry points A and C was 400 cars per hour. From entry point B the traffic flow rate was set to 200 cars per hour, and for entry point D, the traffic flow was set to 200 buses per hour, therefore simulating a bus lane. The average speed of the vehicles travelling through the domain was 14 km/h, reflecting the low speeds in busy urban areas. Each vehicle travelled directly across the crossroads, with no vehicles turning. At the crossroads, a traffic light system was implemented. The traffic lights, seen as green and red lines in Figure 1, allowed traffic to proceed along only one road at any given time. The lights followed a signaling sequence as follows: 26 seconds Green, 3 seconds Amber, 30 seconds Red, 1 second Amber and Red. The first 15 minutes of the traffic simulation was discarded in order to provide Fluidity with a fully developed traffic flow. The UK convention of vehicles driving on the left hand side of the road was adopted.

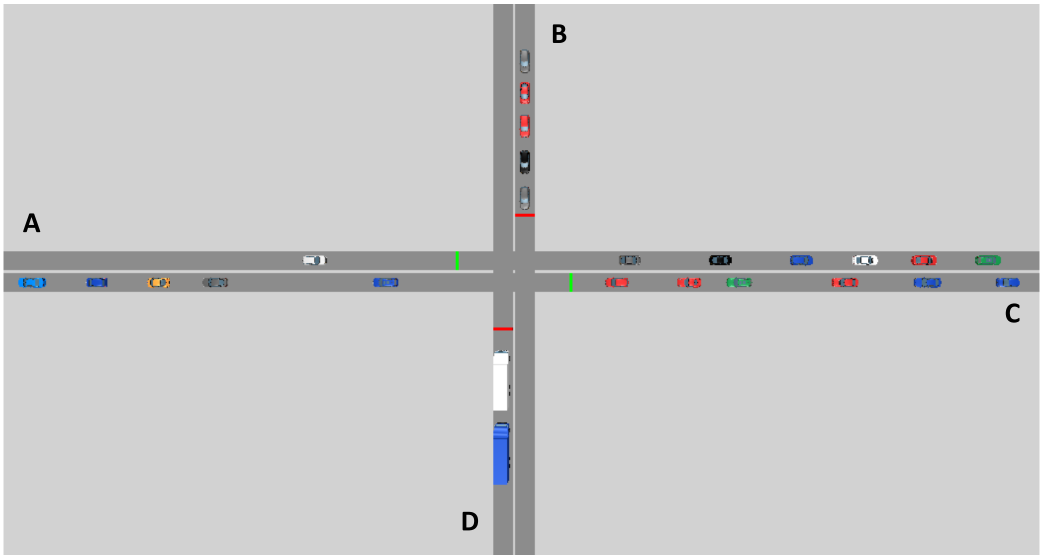

Figure 1: Snapshot of PTV Vissim traffic simulation of a crossroads consisting of three lanes of cars and one bus lane. Red and green lines indicate location of traffic lights. The vehicle colours hold no significance.

The crossroads geometry used in Fluidity is shown in Figure 2, where the crossroads are formed by the intersection of two street canyons orientated at an angle of 45° to the average wind direction. The domain size is 900 m x 800 m x 100 m. The intersecting canyons are formed by the inclusion of four 200 m x 200 m x 10 m buildings separated by 20 m. Each street canyon therefore has a width of 20 m and height of 10 m and both roads have a length of 420 m. The distance from the canyon centerline to each vehicle centerline is 2 m, simulating a road width of approximately 9 m. Each pavement is therefore 5.5 m wide with the exact distance from the canyon walls to the vehicle dependent on whether a car or a bus is considered.

3.2. Boundary conditions

The Synthetic Eddy Method (Jarrin et al. 2006, Pavlidis et al. 2010) is used to apply a turbulent velocity profile at the inlet. A profile representative of a neutral atmospheric boundary layer is applied with a reference velocity of 1.5 m/s at roof height (10 m). A low wind speed was chosen in order to simulate a scenario where traffic movement is likely to be at its most significant and dominates the turbulence production within the canyon. No slip conditions were applied at the floor and building surfaces, "no shear" conditions were applied to the two side walls and top surface and a pressure boundary condition was applied to the outlet. As previously mentioned, a minimum element edge length of 0.5 m was used, along with a maximum edge length of 10 m. The maximum number of nodes allowed for the mesh was set to 1 million, however this number was never reached with the mesh size never exceeding 600,000 nodes. The average element edge length within the canyon was approximately 1 m.

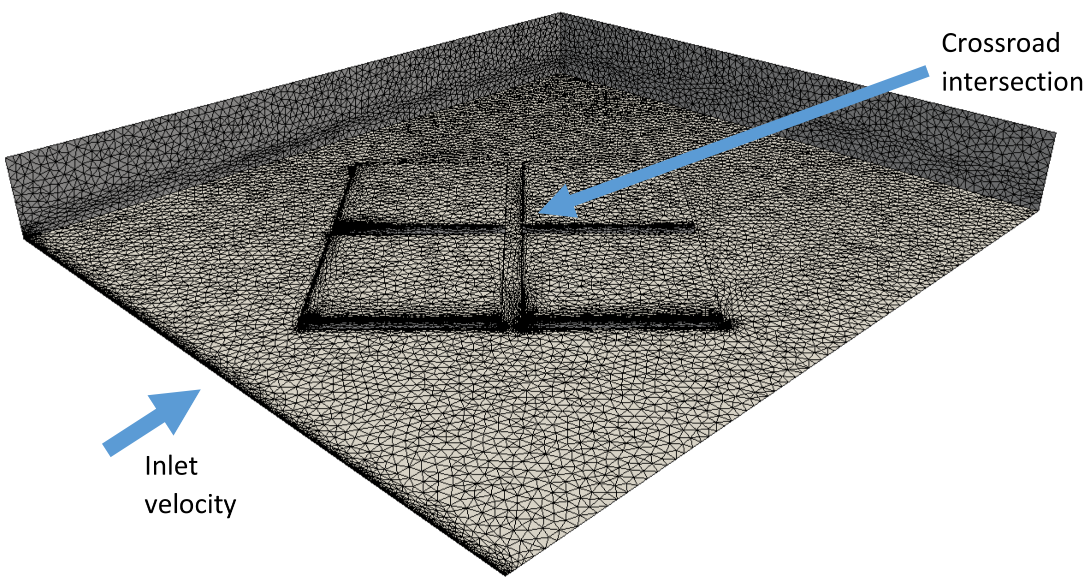

Figure 2: Initial mesh for crossroads geometry

At each time step of the simulation, Fluidity uses the instantaneous emission models described in Section 2.3 to calculate the magnitude of the instantaneous release of emissions from each car and bus. Linear interpolation is used to calculate the vehicle velocity and acceleration at any given time from the 0.5 second resolution input from the traffic simulation. The passive tracer is released at either the rear right-hand or left-hand side of the vehicle with a 50% chance of being either side. For buses, the emissions were always on the left-hand side. These emission volume sources were cubes of 1 m height.

Large emission source volumes were required in order to ensure the presence of a mesh element within the volume and therefore a continuous emission source. These were positioned such that the source lay within the vehicle wake, with the centre of the cube 0.5 m from the vehicle's rear face, 0.5 m from the side of the vehicle and 0.5 m from the ground. The emissions for each lane of traffic was considered as one tracer field, so that the dispersion of emissions from each lane can be independently analysed, allowing for the investigation of the dispersion of emission from one lane by the traffic from another. As there are four lanes of traffic in this simulation, four separate tracer fields are considered. Each tracer field has several moving sources, one at the rear of each of the vehicles in the corresponding lane at that time.

The simulation was allowed to run for 1000 seconds (~16 minutes) before the introduction of traffic in order to develop the street canyon flow. Once traffic was introduced, the first 10 minutes was considered an initialization period, and the remaining 8 minutes involved 8 sets of one-minute traffic light sequences. Thus, the overall simulation time without and with traffic was approximately 34 minutes. The simulation time with traffic was approximately 40 seconds/day running on 16 cores.

3.3. Test Cases

The crossroad simulation with moving vehicles was compared to a crossroad simulation without, using line sources to model traffic emissions. Two line sources were used, which are in reality volume sources extending the length of each of the two roads, with a width of 8m and height of 2m, approximately the width of two traffic lanes and the height of the cars respectively. The emission rate at the intersection of the two volume sources was therefore twice of that elsewhere as the two volume sources overlapped. A schematic of the two simulations is shown in Figure 3.

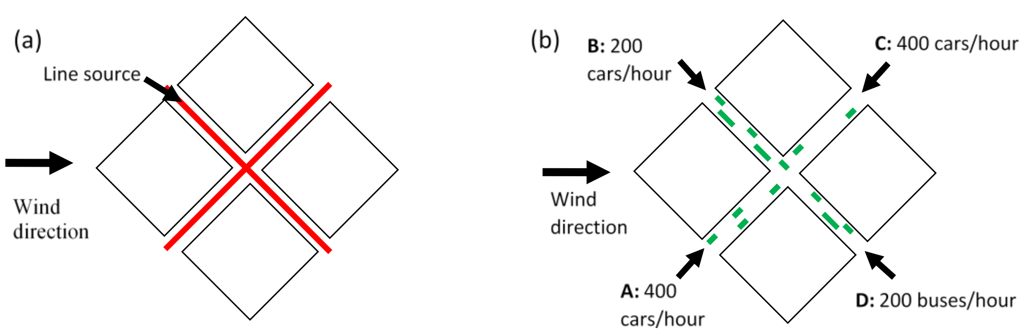

Figure 3: Schematic of (a) the line source simulation and (b) the traffic model simulation.

4. Results and Discussion

4.1. Emissions

Figure 4 (a) and (b) show the instantaneous emissions and velocities for a car and a bus, respectively, as they move through the crossroads domain. The zero velocity period for both cases is due to the period the vehicle spends waiting for the lights to turn green at the crossroads. The large emission peaks during periods of high acceleration are clearly visible and show similar behavior to that presented by O'Driscoll et al. (2016) for measurements taken for a Euro 6 diesel car.

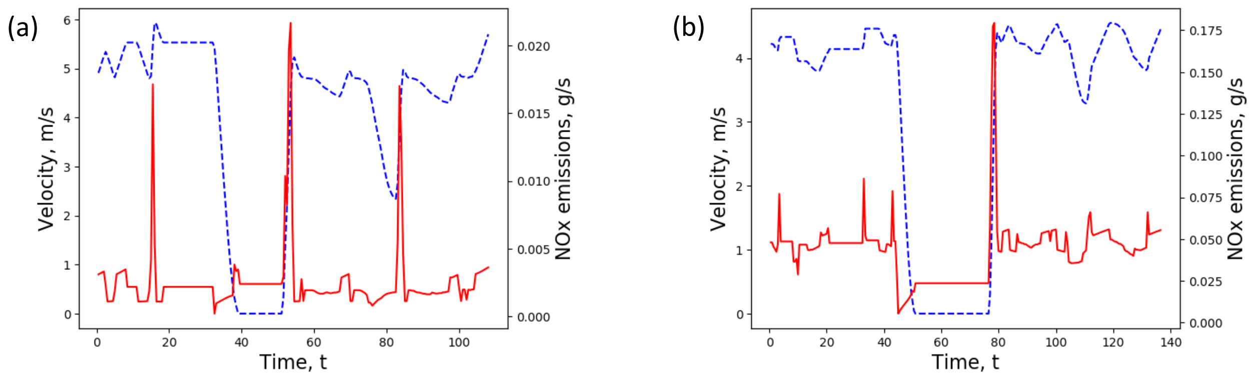

Figure 4: Vehicle velocity (blue, dashed) and NOx emissions (red) against time for (a) a car and (b) a bus moving through the crossroads geometry.

Figure 5 shows the cumulative emissions along each road per meter length of road for the traffic movement simulation for the 8 minute duration analyzed here. It is noted that the emissions model used is based on an old vehicle fleet, however interesting insights can be obtained from looking at the variations in emissions. The average emission factor for the cars travelling through the domain was 0.55 g/km, whereas the average emissions factor for a Euro 6 diesel car driving urban routes is likely to be closer to 0.4 g/km (O'Driscoll et al. 2016). The average emission factors for the buses travelling through the domain were an order of magnitude higher than for the cars. These emission factors, while perhaps higher than the average for a modern fleet, are not beyond reasonable expectation. Further, as the nonlinearity of chemistry is not considered, the concentrations can be scaled to reflect a desired average emission factor.

The emission peaks that can be clearly seen for each lane are at the locations where the vehicles queue at the traffic lights. This region of high emissions is partly due to the emission peaks at acceleration, such as those seen in Figure 4; however they are also due to the accumulation of emissions while the engine is idling and the vehicles are stationary. For this simulation, high emission rates as a result of accelerations contribute between 20-30% to these peaks. The remaining 70-80% is due to emissions that occur during idling. Despite the idling emission rates being significantly lower than the peak emission rates whilst accelerating, the length of time spent idling leads to higher contributions to the total amount emitted. This ratio is likely to be different for more modern vehicles where idling emissions in particular would be expected to be lower.

Comparing the plots for lanes A, B and C, despite the different vehicle counts between each lane, the maximum emission peaks are all similar in magnitude (roughly 1 g/m). This is attributed to the vehicle flow rate being sufficiently high along each road so that at least one vehicle is likely to be waiting at the traffic lights each time they turn red. The lower traffic flow for case B is reflected in the higher rate in decrease of each peak with distance from the crossroads in addition to fewer peaks in total. The emissions away from the crossroads are also lower for case B than for cases A and C where the traffic flows are higher. Case D has significantly higher emissions than the others due to the different emissions model used, representative of an older bus fleet. Case D can also be seen to be a bus lane from the large distance between the emission peaks at the crossroads in comparison to those of the other cases with smaller vehicles. The vehicle count and total NOx emitted during the 8 minute period is shown in Table 2. Lane D is the bus lane and has much higher emissions due to the different coefficients used for the buses as seen in Table 1.

Table 2: Vehicle count and total NOx emitted along each lane of traffic over the 8 minute period.

Lane	A	B	C	D
Vehicles	62	38	51	32
NOx emitted (g)	12.8	8.9	12.0	114.1

In each case, away from the crossroads the accumulated emissions are two orders of magnitude lower than the highest peaks at the crossroad but remain highly variable.

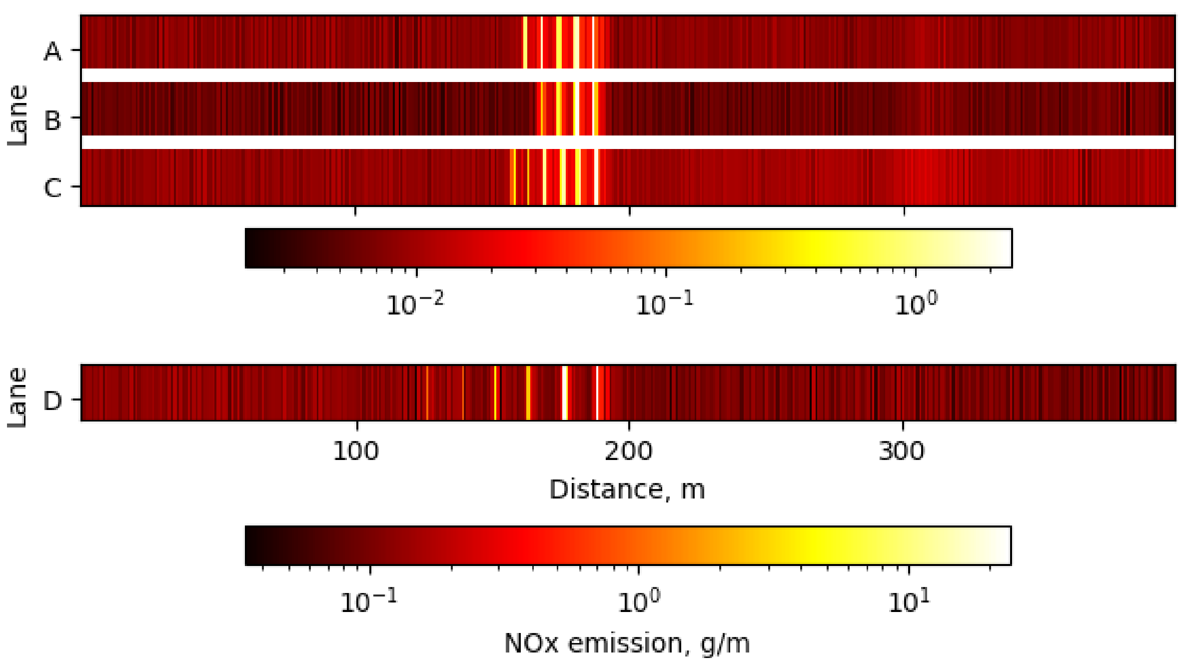

Figure 5: Cumulative emissions per meter of road length for each lane of traffic.

4.2. Velocity fields

Figure 6 shows average velocity fields on a z-plane at a height of 1 m for the line source case, where the velocities are shown for a rotated coordinate system to align with the two street canyons. Figure 6 (a) shows the velocity in the x_{rot} direction, as indicated by the coordinates in the diagram, and Figure 6 (b) shows the velocity in the y_{rot} direction. It is clear that there exists a prevailing flow along both canyons, dictated by the wind direction, driven mainly by the inflow of air at the entrance of the street canyon. Higher velocities are also present immediately downwind of the intersection due to the downwash of air into the intersection which again drives the flow along the canyon.

Figure 7 shows the equivalent average velocity fields for the case with traffic-induced dispersion. These velocity fields are averaged over the 8-minute period. There is a clear difference between the case with traffic-induced dispersion and that without. In contrast to the line source case, there doesn't seem to be an obvious direction of prevailing flow along either canyon when traffic movement is included other than near the wind facing ends of the two canyons where the inflow of air is still significant. This suggests that, at least at this height of 1 m from the ground, the traffic movement has a significant impact on the flow for the low wind speed case considered. This reflects the wind tunnel results of Di Sabatino et al. (2003) where moving plates, representing vehicles, were found to induce a prevailing flow. This wind tunnel setup was simulated using the Fluidity traffic model and good agreement was found between the two as discussed further in Appendix B. In the case of the bus lane, a region of upwind average velocity can be seen in Figure 7 (b). The buses have a larger impact on the air flow within the canyon due to their larger size.

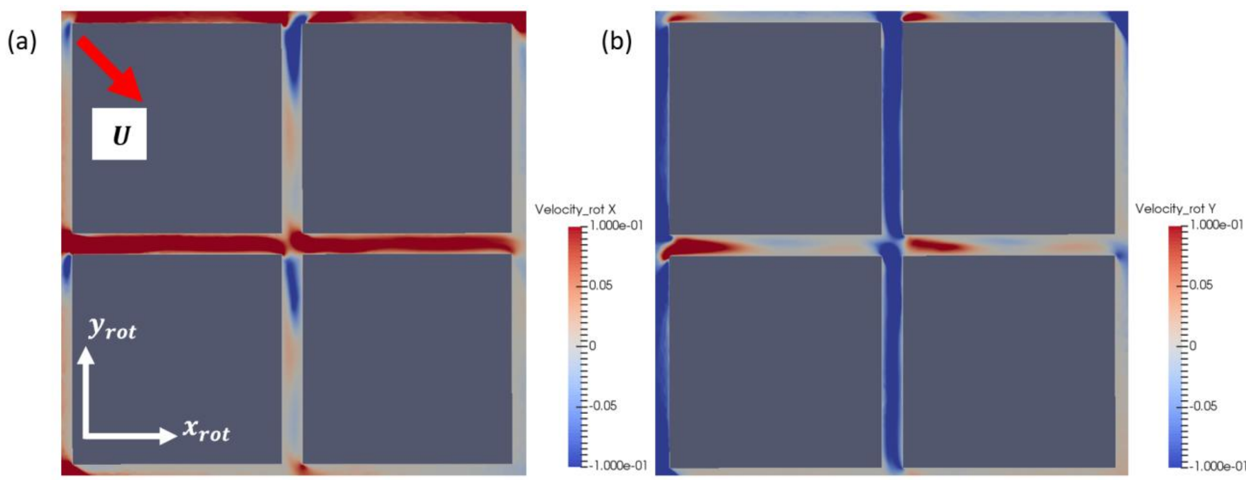

Figure 6: Average velocity field for line source simulation rotated to align with street canyons at a height of z=1m.

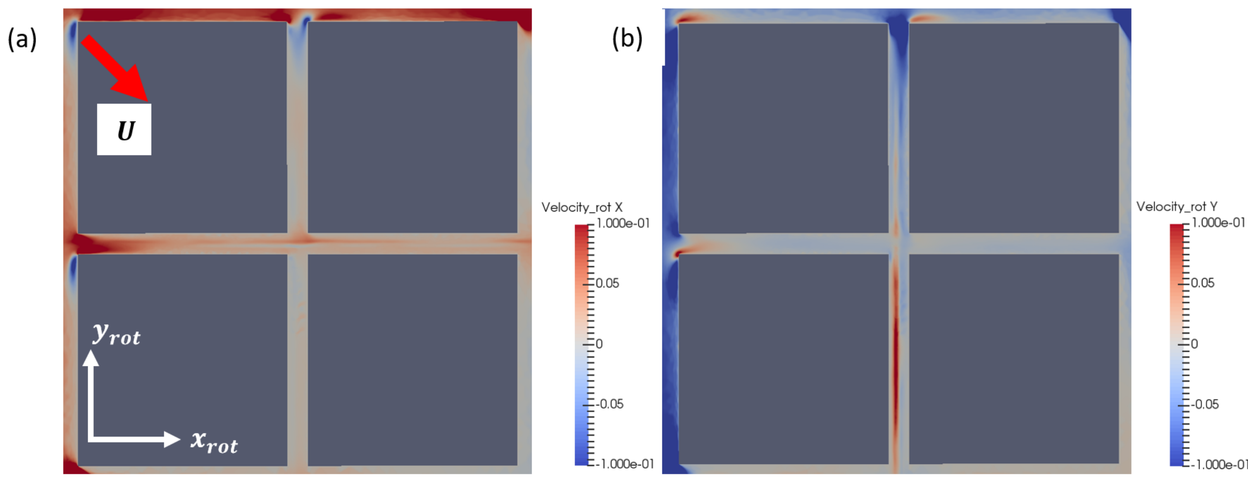

Figure 7: Average velocity fields for traffic simulation rotated to align with street canyons at a height of z=1m.

4.3. Tracer dispersion

Figure 8 shows an instantaneous tracer concentration field for the line source case on a plane at heights z=1 m, 4 m and 8 m. Only one canyon is shown as the concentrations in the two canyons are very similar due to the symmetry of the geometry. The concentrations shown have been scaled using the total emissions of the line source and instantaneous emissions simulations as follows:

$$C_{line}^{*} = C_{line}\frac{E_{traffic}}{E_{line}},$$

where C_{line}^{*} is the scaled concentration, C_{line} is the original concentration due to the line source emissions E_{line}, and $E_{traffic}$ is the total traffic emissions for the simulation period. C_{line}^{*} therefore represents the concentrations due to emissions from a line source equating to the emissions from the traffic-induced dispersion simulation. The effect of the inflow of air at the wind-facing ends of the canyons is clear as the tracer is dispersed down the canyon towards the intersection. This is particularly true higher up the canyon, where concentrations at z=8 m are very low upwind of the intersection. Vertical mixing generated by the inflow of air at the intersection leads to higher concentrations higher up the canyon downwind of the intersection. While a turbulent flow is applied at the inlet, the street canyons are shielded from this turbulence to a degree due to a boundary layer that forms along the flat roofs of the four buildings. This leads to the tracer dispersion at z=1 m being dominated by larger scale turbulent motions generated by the canyon geometry rather than small scale turbulence.

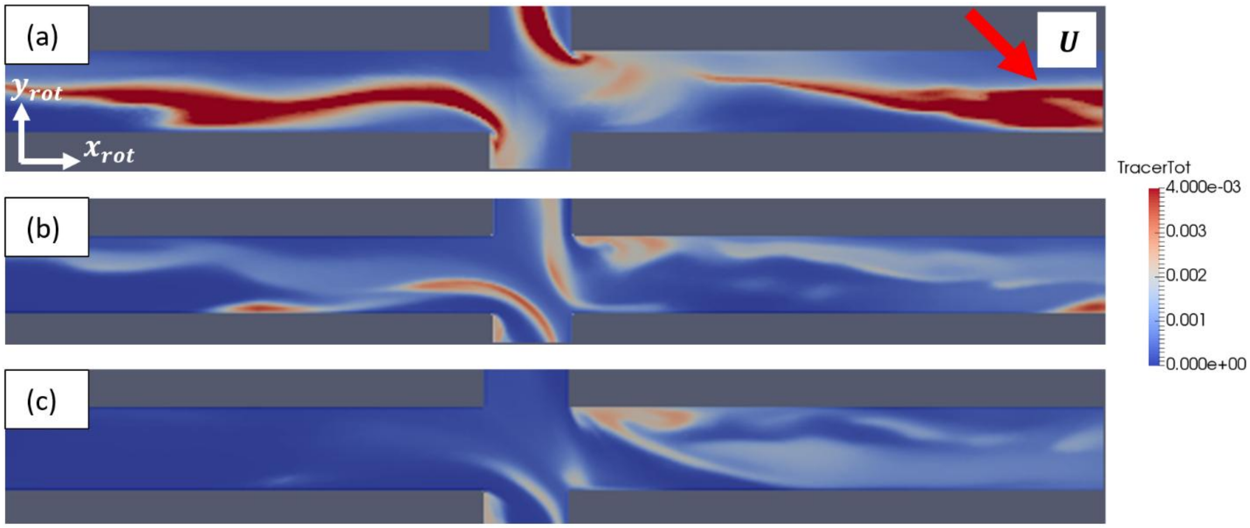

Figure 8: Instantaneous scaled tracer concentrations (g/m^3) for the line source simulation at (a) z=1m, (b) z=4m and (c) z=8m.

Figure 9 and Figure 10 shows an instantaneous concentration field at three different heights for the traffic emissions along canyons A and C and canyons B and D, respectively. Here Figure 10 has been rotated horizontally. The effect of the vehicles on the tracer dispersion is immediately evident. For this particular point in time, the vehicles in lanes B and D are moving across the crossroads while the vehicles in lanes A and C are waiting at the red lights. The higher concentrations behind the buses are due to the higher emission rates for these vehicles. The inclusion of moving vehicles leads to greater mixing of the emissions across the canyons as compared to the line source concentration fields seen in Figure 8. There are also significantly higher concentrations at height z=8 m upwind of the intersection when vehicle movement is included. This is particularly true for the bus lane. The concentration field along the bus lane suggests a highly turbulent flow with significant vertical dispersion.

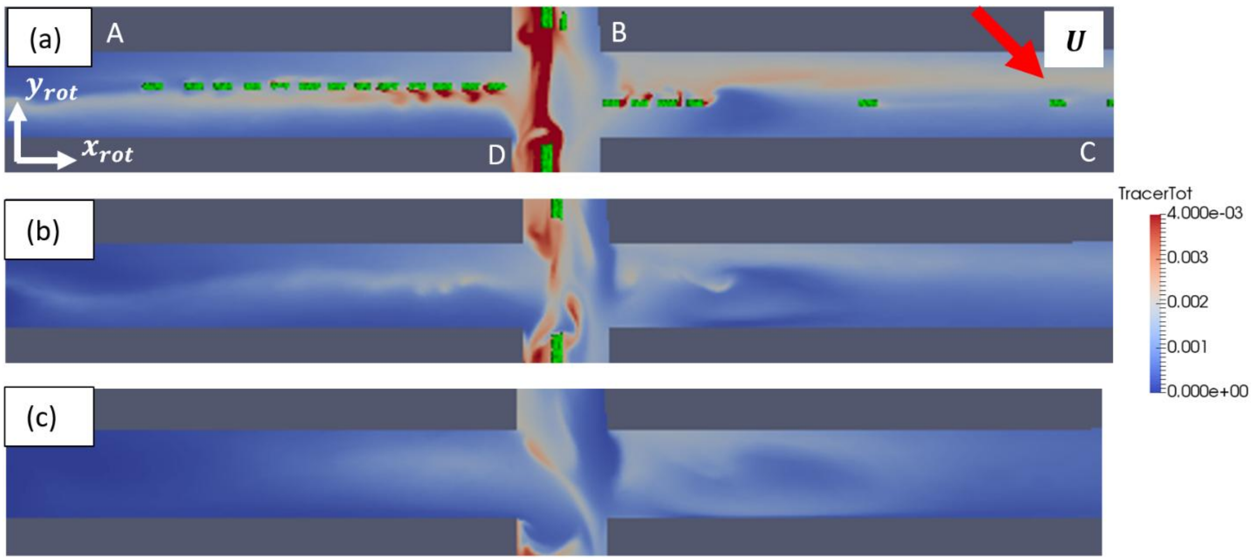

Figure 9: Instantaneous tracer concentration (g/m^3) along lanes A and C due to emissions from all traffic lanes at (a) z=1m, (b) z=4m and (c) z=8m.

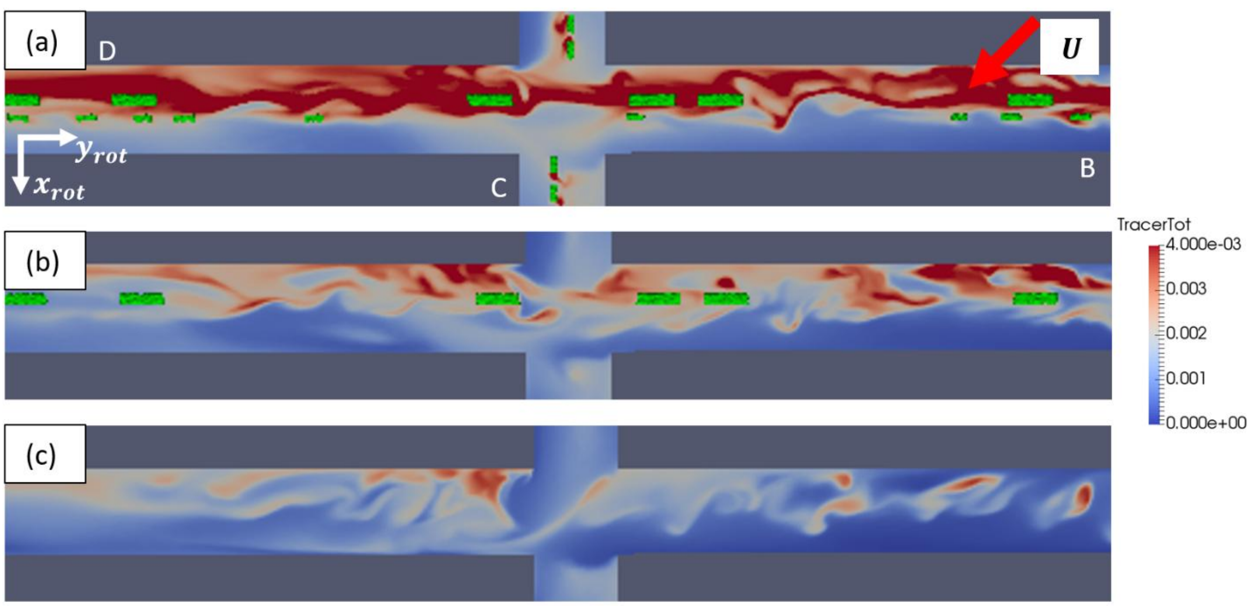

Figure 10: Instantaneous tracer concentration (g/m^3) along lanes B and D due to emissions from all traffic lanes at (a) z=1m, (b) z=4m and (c) z=8m.

As the bus emissions are significantly greater than those of the cars, a clearer picture of the situation can be obtained by analysing the emissions from the cars and the buses separately. Figure 11 shows the emissions from the cars only (i.e. lanes A, B and C) at four different times. Arrows are used to show which lanes are moving across the intersection and a red cross is used to indicate a red light for that lane, with each lane corresponding to the symbol to its clockwise direction. An amber arrow indicates that the lights are about to turn red, while the green arrow cases show the situation shortly after the light turns green.

In Figure 11 (a), lanes B and D have been moving across the intersection for the green light period of 26 seconds, and the lights are about to turn red. Meanwhile, the vehicles in lanes A and C have been idling for this 26 second period while waiting for the lights to turn green. The build up of emissions due to the idling vehicles is clear to see. The emissions from the idling vehicles in lane A are not dispersed across the intersection by the prevailing in-canyon wind direction due to the perpendicular flow generated by the passing buses. Instead, concentrations build up across the street ahead of the queueing vehicles, where you may expect to find waiting cyclists and pedestrains.

In Figure 11 (b) the vehicles in lanes B and D have now stopped and the vehicles in lanes A and C are moving across the intersection. The concentration hotspot that formed ahead of the qeueing vehicles in lane A seen in Figure 11 (a) is now dispersing across the intersection. High concentrations are present behind the cars as they accelerate across the intersection and entrain some of the emissions built up while idling.

In Figure 11 (c) the cars in lane A and C have been moving across the intersection for the duration of the green light period. High concentrations are clearly seen within the wake of the two lines of traffic, with higher emissions in lane A due to a higher volume of traffic at this time. In Figure 11 (d), lanes A and C have stopped and lanes B and D are now moving across the intersection, clearing away the emissions due to lanes A and C as they do so. The shear layer blocking the dispersion of the idling emissions seen in Figure 11 (a) forms again as the buses cross the intersection. High concentrations can be seen behind the cars in lane B due to the period spent idling.

Figure 12 shows the the bus emissions for the same period as Figure 11. In Figure 12 (a) the buses have been moving across the intersection for the duration of the green light period. The bus emissions are contained within the wake of the buses to a greater extent than for the cars due to the larger size of the vehicles leading to a stronger wake. It can be seen in Figure 12 (b) and (c) that as the cars move across the intersection they clear away the bus emissions from the intersection. In Figure 12 (c) the emissions due to the idling buses are dispersed in the direction of travel of the buses, which is upwind relative to the in-canyon wind direction. This is despite the buses having been stationary for up to 26 seconds, however as shown in Figure 7 (b), the bus lane induces an upwind flow within the canyon. Figure 12 (b) and (c) also show that as the buses decelarate the high emissions within their wakes are dispersed across the street leading to high concentrations on each side of the street where pedestrians are likely to be walking. High concentrations are again seen in Figure 12 (d) as the buses accelerate once the light turns green.

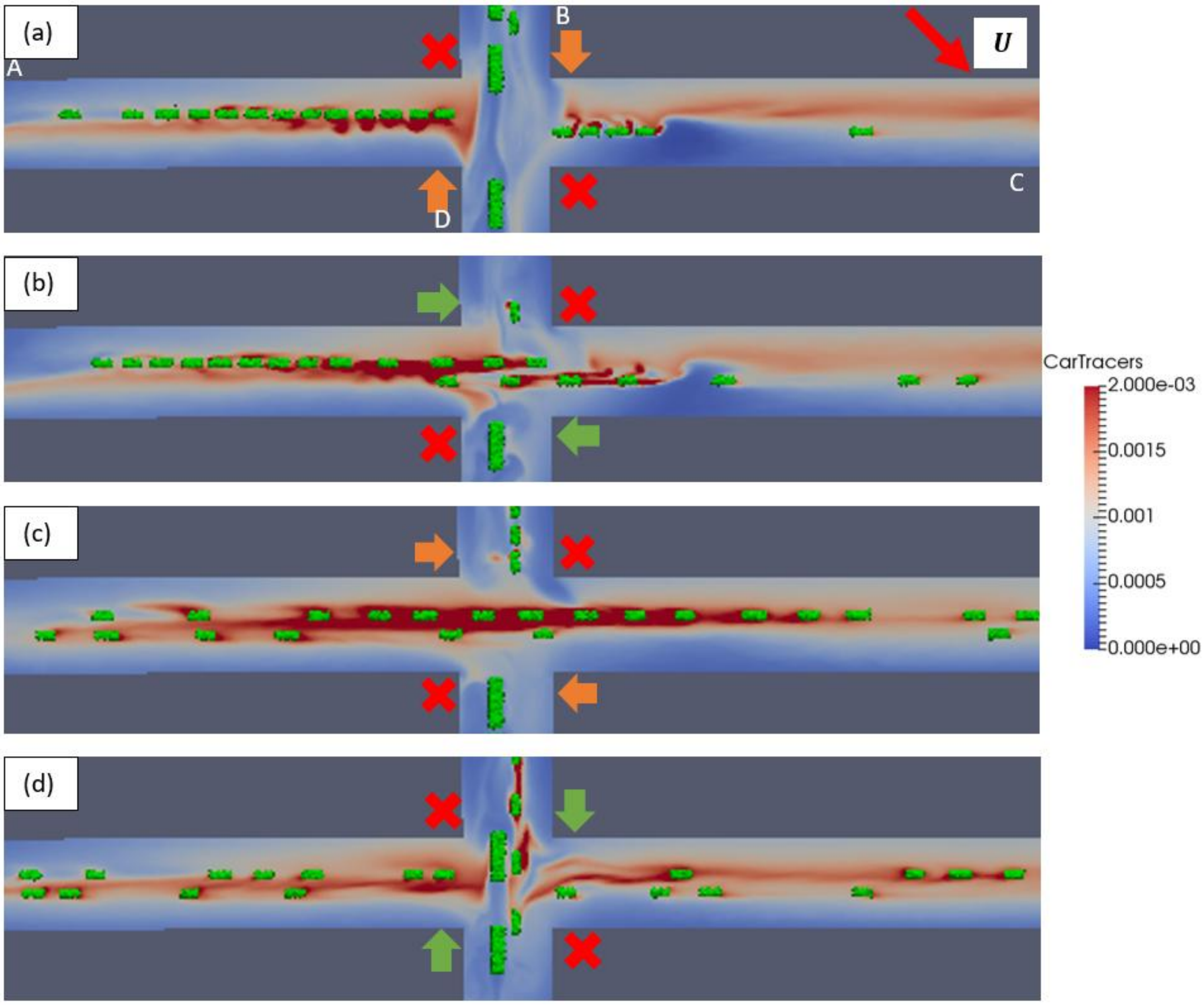

Figure 11: Tracer concentrations (g/m^3) due to emissions from lanes A, B and C at a height of z=1m at different stages of the traffic lights signaling.

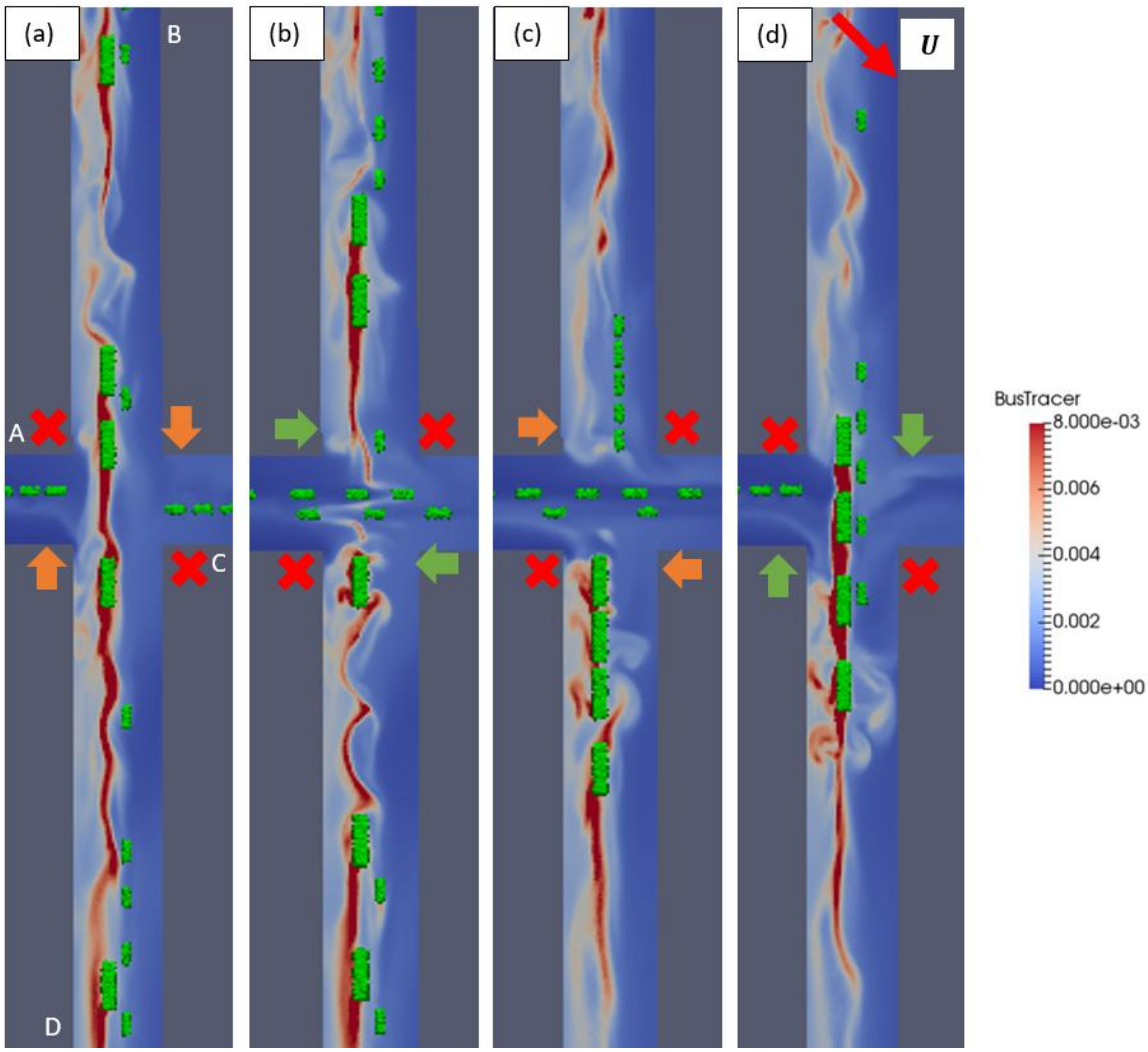

Figure 12: Tracer concentrations (g/m^3) due to emissions from lane D at a height of z=1m at different stages of the traffic lights signaling.

Figure 13 (a) and (b) show the tracer concentration fields for the emissions from lanes B and D, and lanes A and C, respectively. A different scale is used to highlight the dispersion of emissions from one canyon to the other. In both cases a larger amount is dispersed in the downwind direction, however significant upwind dispersion of emissions from the intersecting road can also be seen.

The crossroads geometry can be considered as four street canyons linked by the intersection at the centre. These street canyons are 10 m high, 20 m across and 200 m long. Denoting each canyon by the lane of traffic which first enters the canyon, we have street canyons SC_A, SC_B, SC_C, and SC_D. Table 3 shows the contribution of each lane of traffic to the total NOx in each of these street canyons. It can be seen that canyon SC_D contains the highest total NOx. This is to be expected as the buses travel along this canyon and it is downwind of the intersection. Similarly, canyon SC_C contains more NOx than canyon SC_A due to its downwind position relative to the intersection. The bus emissions contribute significantly to the total NOx in each canyon, including canyons SC_A and SC_C along which no buses travel. This is true for canyon SC_A (19.5%) despite its upwind location relative to the intersection as the vehicles travelling along lane C entrain the bus emissions as they pass over the intersection. This demonstrates how concentrations along quieter roads could be significantly increased by the entrainment of pollutants from busier intersecting roads.

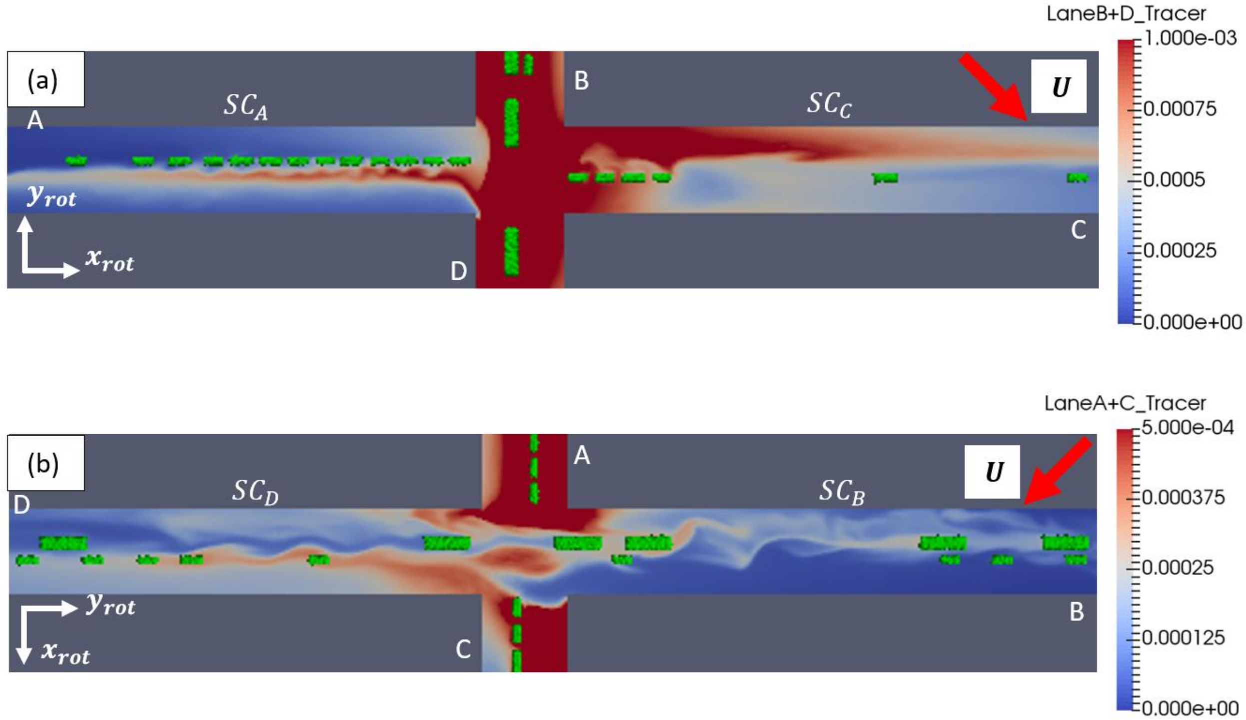

Figure 13: Tracer concentrations (g/m^3) in (a) canyons SC_A and SC_C due to emissions from lanes B and D and (b) canyons SC_B and SC_D due to emissions from lanes A and C. Emissions from each canyon are dispersed in both the downwind and upwind directions along the intersecting canyon.

Table 3: Contribution from each traffic lane to total NOx in each canyon.

	Grams of NOx in canyon due to lane emissions				
Canyon	Lane A	Lane B	Lane C	Lane D	Total
SC_A	6.7 (35.8%)	0.4 (2.1%)	7.9 (42.6%)	3.6 (19.5%)	18.6
SC_B	1.0 (2.3%)	2.8 (6.2%)	0.9 (1.9%)	40.5 (89.7%)	45.2
SC_C	14.1 (31.7%)	2.4 (5.4%)	11.2 (25.2%)	16.7 (37.7%)	44.3
SC_D	3.3 (5.1%)	6.2 (9.5%)	3.9 (5.9%)	52.0 (79.6%)	65.3

4.4. Roadside concentrations

Four locations were chosen to investigate the effect of traffic on the variation in concentration levels seen at the intersection. These locations are shown in Figure 14. The points were chosen as locations where pedestrians and cyclists may be expected to wait to cross the intersection. The points are approximately 2 m from the nearest passing lane of traffic.

Figure 15 shows box plots of the concentrations seen at points 1 to 4 for the line source model and the traffic-induced dispersion model. For the line source model, the median concentration varies significantly between each location, with the median at point 2 over 11 times higher than that at point 1. From Figure 8 it can be seen that point 2 is located in an area of high concentration formed by the dominant in-canyon wind flow. However, for the case with traffic movement the median concentrations are more consistent between each location, with the highest median, at point 4, less than twice that of the lowest, at point 3. This lower variation between the median concentrations relative to the line source model at points 1 to 4 is perhaps unexpected considering the different distances of each point to the higher polluting bus lane and suggests that the moving vehicles are effective in mixing the emissions at the crossroads.

The variation in concentrations at each point is also affected by the inclusion of traffic-induced dispersion. The variation is increased at point 4, with an increase in the relative standard deviation (RSD) from 0.29 for the line source to 0.72 with moving vehicles. Here we define the RSD as the standard deviation, σ, over the mean, μ, such that $RSD = \sigma/\mu$. Despite the use of an instantaneous emissions model, at points 1 and 3 the RSD is lower with the traffic dispersion model, at 0.06 and 0.13, respectively, in comparison to 0.45 and 0.26, respectively, for the line source model. The RSD at point 2 is in relative agreement for the two models. With the inclusion of traffic-induced turbulence and instantaneous emissions, point 4 experiences peak concentrations up to seven times greater than the median. Point 4 is next to the bus lane and close to where the buses accelerate from standstill when crossing the intersection. Higher concentrations are to be expected here relative to points 1, 2 and 3 due to the higher emission rates for the buses. However the larger variation relative to the mean seen at this point cannot be explained by the higher emissions alone as comparable RSD values would also be expected at points 1, 2 and 3. Rather, the high RSD (0.72) and high number of outliers at point 4 is due to the impact of the buses on the airflow as they drive past as seen in Figure 12. It can be seen from Figure 12 that bus emissions tend to stay within the strong wake of the bus rather than disperse more smoothly across the street as is the case for the car emissions in Figure 11. This leads to high concentration gradients within the street. As the buses decelerate to stop for the lights, these areas of high concentrations behind the buses are dispersed to the side of the road (as seen in Figure 12), leading to the exposure of pedestrians and cyclists to large concentration peaks.

These results indicate that if the exposure of pedestrians and cyclists is to be modelled accurately, exposure to acute concentration events must be considered. Let us estimate the exposure at any point as $E_{NO_x} = \sum_i C_i t_i$, where C_i is the concentration at time t_i. At point 4, the top quartile (i.e. highest 25%) of concentration values contribute to 48% of the overall exposure yet only occur for 23% of the total time. Whereas the contributions of the outliers only, that is the values that exceed the upper quartile plus 1.5 the interquartile range, contribute to 18% of the exposure and only 6% of the total time. These outliers are therefore likely to contribute significantly to the exposure of pedestrians and cyclist while waiting to cross the intersection. Although this analysis uses stationary points, while cyclists and pedestrians will move across the intersection, it demonstrates the extent to which acute concentration events can contribute to overall exposure. This is particularly significant for cyclists who have higher inhalation rates and often share road space with buses.

While this simulation represents one theoretical scenario, with a constant wind direction, the method could be used for in depth analysis of pedestrian exposures at busy junctions.

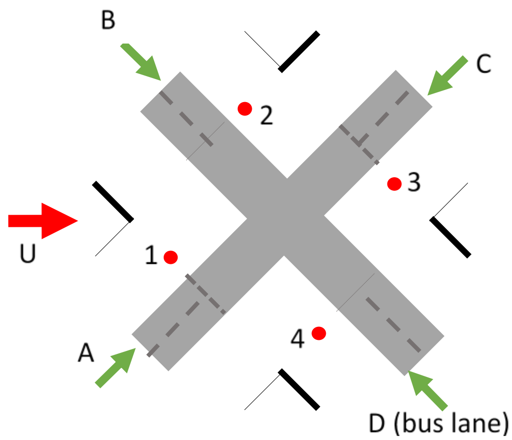

Figure 14: Location of points chosen for exposure analysis. Locations 1 to 4 are at a distance of 2 m from the nearest lanes of traffic.

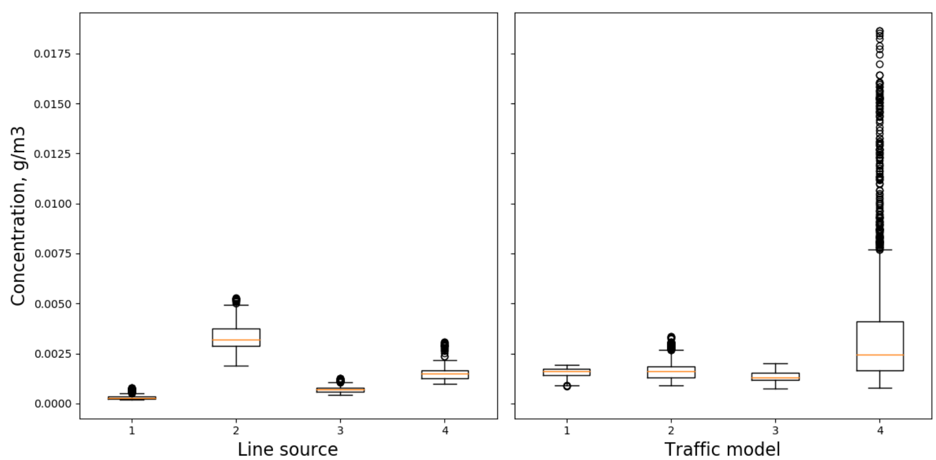

Figure 15: Box plots of NOx concentrations at points 1-4 for the line source and traffic model. The lines show median values, the boxes represent the interquartile range and the whiskers (lines extending from the box) extend to the first point within 1.5 times the interquartile range.

5. Conclusions

An idealized crossroads geometry is simulated using the CFD code Fluidity. The dispersion of pollutants is modelled in two ways: firstly wind driven dispersion using a line source to represent traffic emissions, and secondly using Fluidity's traffic model to capture traffic inducted dispersion of instantaneous emissions. A low wind speed case is simulated in order to investigate a scenario where the impact of vehicle movement is likely to be at its most significant and dominates the turbulence within the canyon. For the second case, the emissions of each lane of traffic is simulated using individual passive tracers, with the emission rate of each vehicle calculated instantaneously as a function of the vehicle's velocity and acceleration. The emission model therefore captures emission peaks during high acceleration. A traffic simulation (PTV Vissum) is used to simulate the traffic flow dynamics which are used as an input to the Fluidity traffic model. A coarse mesh relative to vehicle size is used, with a minimum edge length of 0.5 m, to limit the long run time required. Despite the low mesh resolution relative to vehicle size, the method is still capable of simulating the effect of vehicles on pollution dispersion as demonstrated by the validation studies presented in the appendix. This is a first attempt at using this method coupled with traffic emissions to look at the dispersion of traffic emissions in an urban scenario. Further work is required to reduce the run times of the simulation and to update the emissions model.

Comparison of the line source and traffic-induced dispersion simulations demonstrate the importance of considering traffic induced flow and the dispersion of emissions by vehicles, along with instantaneous emission rates, when considering urban concentrations. We observe that the inclusion of traffic movement has an impact on the prevailing direction of air flow near ground level for this low wind speed scenario, leading to notably different concentration fields to that given by the line source simulation with no traffic movement. The traffic simulation demonstrates the ability of vehicles to disperse emissions from other sources upwind and provides insights into the formation of pollution hotspots at the intersection. The inclusion of moving vehicles and instantaneous emissions model has a significant impact on the estimation of exposure of pedestrians and cyclists, particularly when large vehicles such as buses are present. For the test case used here, it is shown that for a roadside location at the intersection 2 m from the bus lane (point 4), the top quartile of concentration values contribute to 48% of the overall exposure yet account for only 23% of the total time. Similarly, the contribution of extremely high concentration outliers, that is the values that exceed the upper quartile plus 1.5 the interquartile range, contribute to 18% of the exposure while accounting for only 6% of the total time. These acute high concentrations are not seen when the effect of traffic movement and instantaneous emissions are not simulated. While these results are taken from a single simulation with a low wind speed and one particular direction and therefore cannot be generalized, they serve as an example of the importance of considering such effects in a typical urban scenario. Further, these results highlight the limitations of using a line source to represent traffic emissions which are highly variable along the road.

The method presented in this paper can be used for detailed exposure analysis of pedestrians and cyclists travelling through urban scenarios. The method is able to resolve the heterogeneous nature of pollution dispersion within streets at high temporal and spatial resolution, therefore resolving the high concentration peaks seen during measurement studies. In order to improve the accuracy of the estimated exposure of active commuters these peak concentrations must be considered. The method can also be used to improve our understanding of the effect of traffic movement on street level flow features in urban areas and to improve the accuracy of simpler operational dispersion models.

Acknowledgements

This work was funded by the Engineering and Physical Sciences Research Council (EPSRC) Grand Challenge grant ‘Managing Air for Green Inner Cities (MAGIC) [grant number EP/N010221/1].

Appendix A – Single vehicle simulation

The single vehicle simulations consisted of single stationary car, modelled using the traffic model described in Section 2, within a domain with a constant inlet and moving floor. This setup was designed to simulate the flow over a vehicle at zero wind conditions.

The inlet velocity and floor velocity were set to 5 m/s in order to produce an equivalent simulation to a vehicle moving at 5 m/s through a zero velocity flow field. The car size was the same as that used for the crossroads simulation and the minimum edge length was set to 0.5 m.

Comparisons were made with two higher resolution simulations. These simulations were of the same setup, however a physical, no-slip boundary was used to model the car rather than the traffic model. The first of these simulations represented the car as an Ahmed body (Ahmed, 1981), the geometry of which can be seen in Figure 16. The approaching wind velocity and floor velocity was set to 5 m/s. The second simulation attempted to replicate the geometry used in wind tunnel experiments by Carpentieri et al. (2012) (a 2004 Vauxhall AstraVan). While the Ahmed body model was full scale, as was the crossroads simulation, the AstraVan model was a 1:20 model in order to replicate the wind tunnel setup. The same velocity used in the wind tunnel experiment of 2.5 m/s was also used here. The minimum edge lengths for these simulations was set to $\sqrt{A}/20$ where A is the cross-sectional area of the surface facing the flow. For the full scale case, this results in a minimum edge length of 0.075 m. These mesh size for these higher resolution simulations was approximately 100,000 nodes in comparison to 20,000 nodes for the low resolution vehicle model.

A passive tracer is emitted from the rear right-hand side of the vehicle at a constant emission rate for each of the three simulations

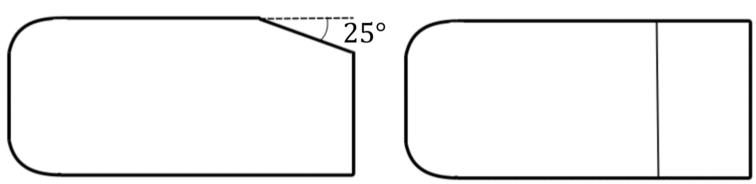

Figure 16: Schematic of Ahmed body shape used for single vehicle simulation.

Figure 17 and Figure 18 are vector plots of the average velocity around the vehicles. It can be seen that despite the low resolution, the traffic model is able to capture the recirculation region behind the car. However the full complexity of the flow is not resolved due to the relatively large minimum edge length used.

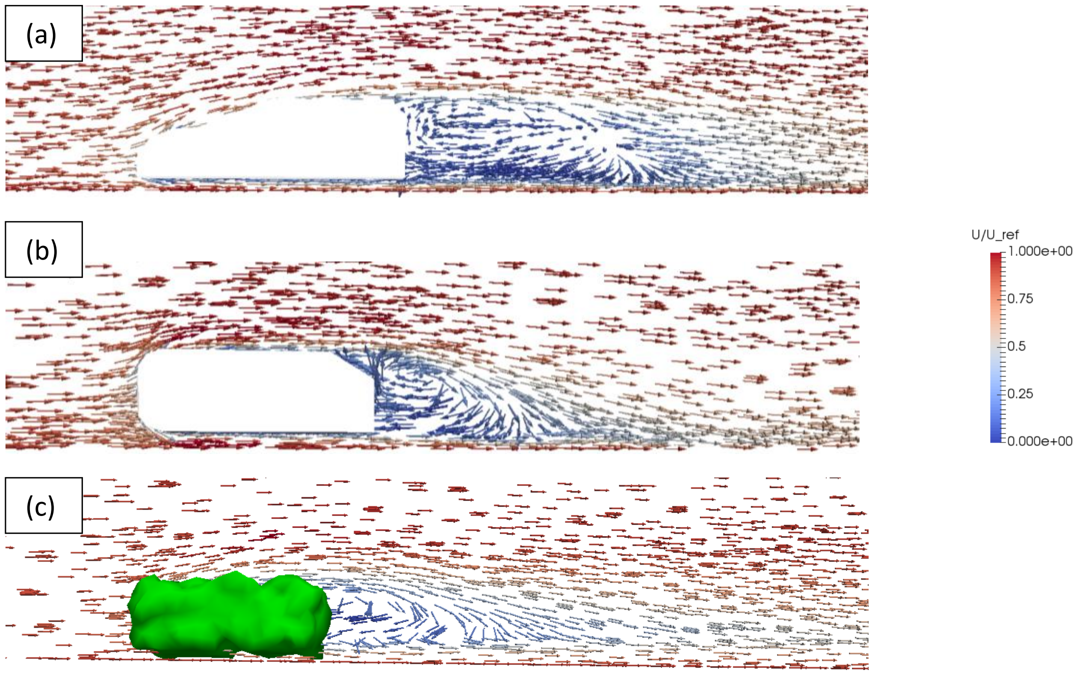

Figure 17: Flow profile on y=0 plane for (a) the AstraVan (b) the Ahmed body and (c) the low resolution vehicle model

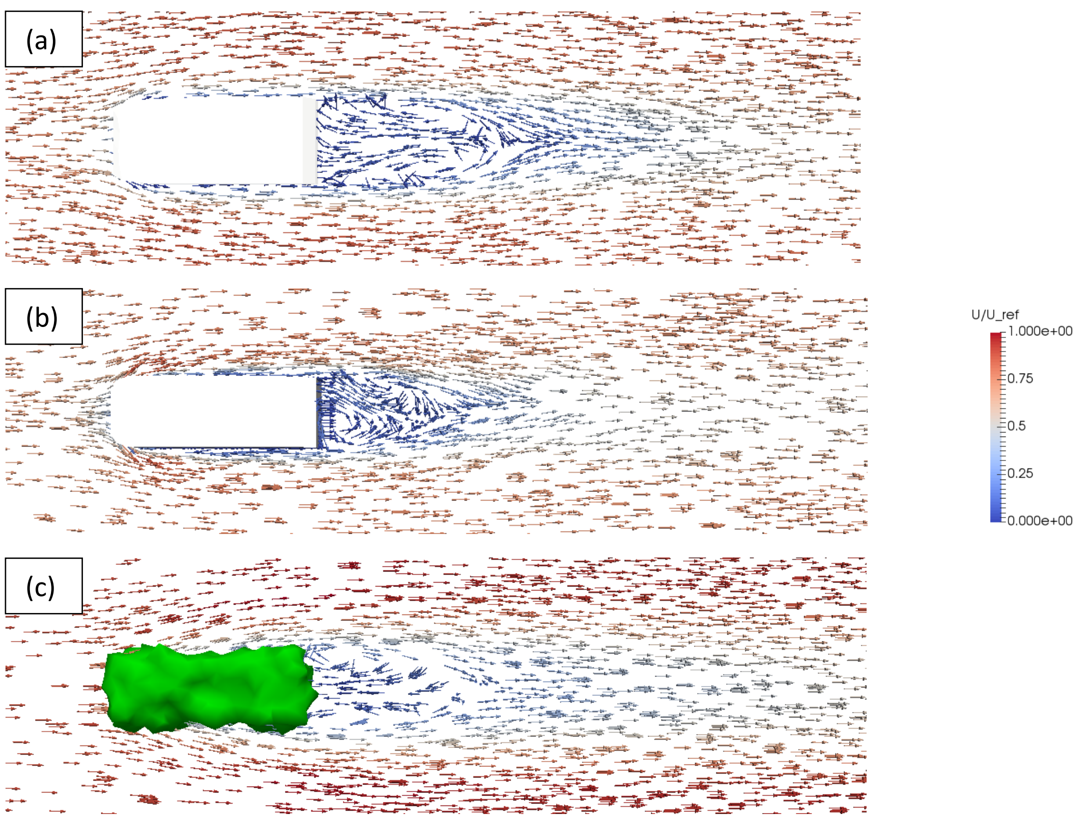

Figure 18: Flow profile on z=0.5m plane for (a) the AstraVan (b) the Ahmed body and (c) the low resolution vehicle model

Figure 19 show a comparison between the vehicle model, the wind tunnel experiment of Carpentieri et al. (2012) and the AstraVan Fluidity simulation for normalized exhaust tracer concentration, C^{*}. Here we define $C^* = (C\ U\ h^2)/Q$, where C is the concentration, U is the approaching wind speed, h is the height of the vehicle and Q is the source mass flow rate. Differences in the profiles are to be expected for the low resolution traffic model, particularly in the near-wake region, as no attempt is made to replicate the shape of the AstraVan. There are also differences between the wind tunnel setup and that used in Fluidity. In the wind tunnel, the AstraVan model is positioned on a false floor above the ground of the wind tunnel and the tracer is released at a velocity of 0.13 times the inlet velocity. For the Fluidity simulations a moving floor is used and a zero-velocity tracer release. However, the objective for the low resolution model is not to perfectly replicate the flow pattern around each vehicle. Particularly as these profiles will vary from vehicle to vehicle due to different shapes and sizes. The low resolution traffic model is capable of providing an estimation of the impact of a typical vehicle on the dispersion of emissions as it moves through a domain. Further work is required to determine the optimal shape and size to represent the average car in the fleet.

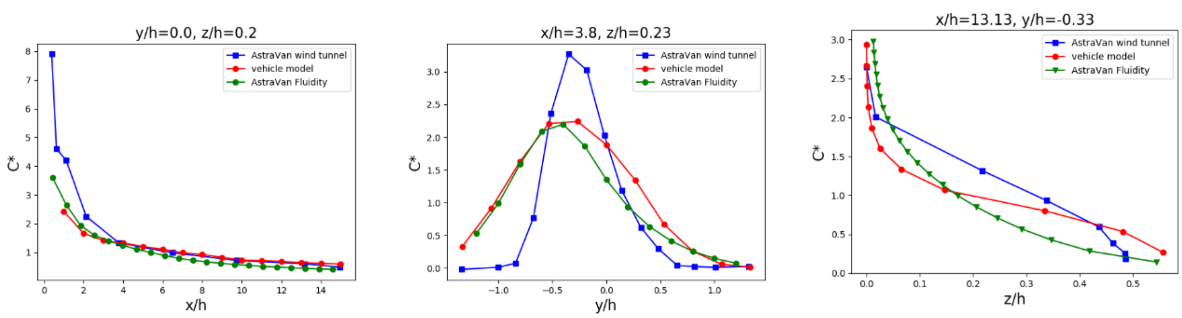

Figure 19: Comparison of low resolution vehicle model with wind tunnel model of Carpentieri et al. (2012) and AstraVan Fluidity simulation.

Appendix B – Traffic induced turbulence for multiple vehicles

In order to assess the performance of the model when considering multiple vehicles, the wind tunnel experiment of Di Sabatino et al. (2003) was simulated. The wind tunnel experiment used moving metal plates on two belts to represent two lanes of vehicles moving along a street canyon in opposite directions, with no prevailing wind flow (i.e. zero wind conditions). A plate density of 20 m^{-1} was used with the plates moving at 12 m/s, representative of a vehicle speed of 30 km/h in full scale. The street canyon was 120 cm long, and had equal height and width of 12 cm. This setup was simulated using the Fluidity traffic model. Rather than using plates, the vehicle dimensions were kept as those used for the crossroad simulation however scaled down to wind tunnel size, with a ratio of 240:1 from full size to wind tunnel scale. A mesh of approximately 600,000 nodes was used, with a minimum edge length of 1.5 mm, equivalent to 0.5 m in full scale as was used for the crossroads test case. This resulted in an average edge length within the canyon of approximately 3.4 mm which at full scale is equivalent to 0.8 m. As for the crossroads simulation, a maximum Courant number of 5 was used to govern the size of the time step. 35 vehicles travelled along each lane during the averaging time.

Figure 19 shows the along-the-canyon and transverse components of the average velocity field while Figure 20 shows the along-the-canyon and transverse turbulent velocities. The values are normalized by the vehicle velocity. A qualitative comparison with the results of Di Sabatino et al. shows that the model provides reasonable approximation of the impact of the vehicles on the prevailing flow directions. The magnitude of the prevailing along-the-canyon flow induced by the vehicles is comparable for the simulation and wind tunnel, with a maximum value around 25% of the vehicle velocity reported by Di

Sabatino et al. Similarly, the transverse component is of similar magnitude for the two cases with both an order of magnitude lower than the along-the-canyon flow. The along-the-canyon and transverse turbulent velocities are also similar for the traffic model and the wind tunnel, with magnitudes up to 15% of the vehicle velocity for the along-the-canyon turbulent velocity, and slightly lower values for the transverse velocity.

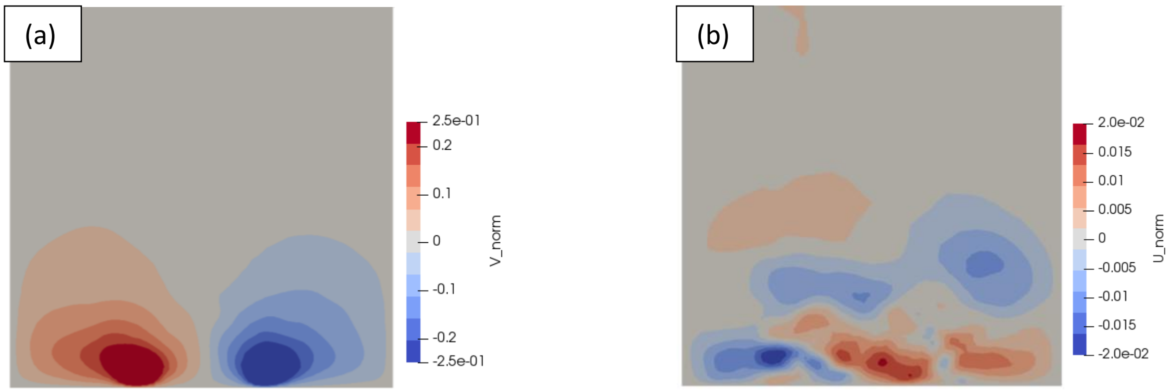

Figure 20: Traffic-produced normalised mean (a) along-the-canyon and (b) transverse velocity component in the central plane of an idealised street canyon.

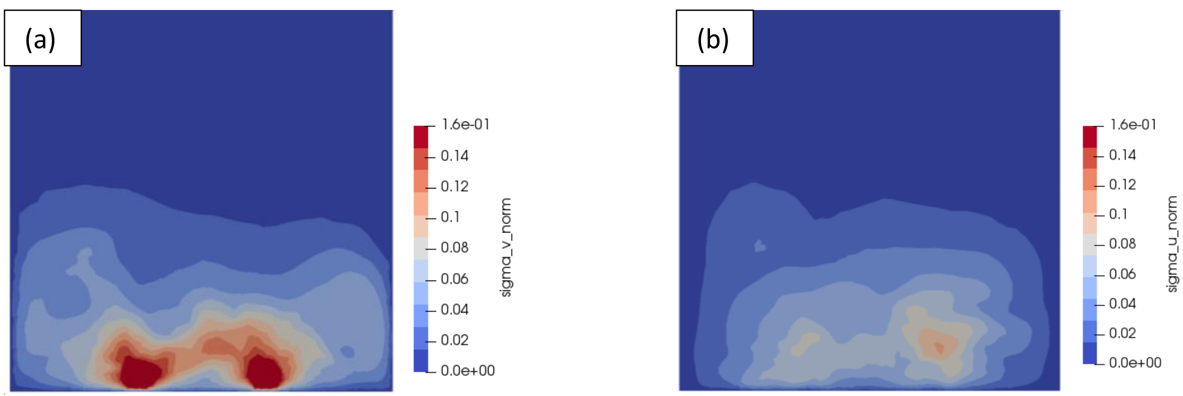

Figure 21: Traffic-produced normalised mean (a) along-the-canyon and (b) transverse turbulent velocity component in the central plane of an idealised street canyon.

References

SR Ahmed, 1981. An experimental study of the wake structures of typical automobile shapes. Journal of Wind Engineering and Industrial Aerodynamics. 9. 49-62.

SJ Arnold, H ApSimon, J Barlow, S Belcher, M Bell, JW Boddy, R Britter, H Cheng, R Clark, RN Colvile, S Dimitroulopoulou, A Dobre, B Greally, S Kaur, A Knights, T Lawton, A Makepeace, D Martin, M Neophytou, S Neville, M Nieuwenhuijsen, G Nickless, C Price, A Robins, D Shallcross, P Simmonds, RJ Smalley, J Tate, AS Tomlin, H Wang, P Walsh, 2004. Introduction to the DAPPLE Air Pollution Project. Science of The Total Environment, 332, 139–153. doi:10.1016/j.scitotenv.2004.04.020

CJ Baker, 2001. Flow and dispersion in ground vehicle wakes. Journal of Fluids and Structures. 15. 1031-1060. doi:10.1006/jfls.2001.0385

P Berghmans, N Bleux, L Int Panis, VK Mishra, R Torfs, M Van Poppel, 2009. Exposure assessment of a cyclist to PM10 and ultrafine particles. Science of the Total Environment. 407. 12860-1298.

JHT Bentham, 2003. Microscale modelling of air flow and pollutant dispersion in the urban environment. Ph.D. Thesis, Imperial College London.

M Carpentieri, P Kumar, A Robins, 2010. An overview of experimental results and dispersion modelling of nanoparticles in the wake of moving vehicles. Environmental Pollution. 159. 685-693.

M Carpentieri, P Kumar, A Robins, 2012. Wind tunnel measurements for dispersion modelling of vehicle wakes. Atmospheric Environment. 62. 9-25.

S Di Sabatino, P Kastner-Klein, R Berkowicz, RE Britter, E Fedorovich. 2003. The Modelling of Turbulence from Traffic in Urban Dispersion Models – Part I: Theoretical Considerations. Environmental Fluid Mechanics. 3. 129-143.

A de Nazelle, S Fruin, D Westerdahl, D Martinez, A Ripoll, N Kubesch, M Nieuwenhuijsen, 2012. A travel mode comparison of commuters' exposures to air pollutants in Barcelona. 59. 151-159.

A de Nazelle, E Seto, D Donaire-Gonzalez, M Mendez, J Matamala, M J Nieuwenhuijsen, M Jerrett, 2013. Improving estimates of air pollution exposure through ubiquitous sensing technologies. 176. 92-99.

CC Daigle, DC Chalupa, FR Gibb, PE Morrow, G Oberdörster, MJ Utell, MW Frampton, 2003. Ultrafine particle deposition in humans during rest and exercise. Inhalation Toxicology. 15. 539-552.

G Dong, TL Chan 2006. Large eddy simulation of flow structures and pollutant dispersion in the near-wake region of a light-duty diesel vehicle. Atmospheric Environment. 40. 1104-1116.

J Dong, Y Tao, Y Xiao, J Tu, 2017. Numerical simulation of pollutant dispersion in urban roadway tunnels. The Journal of Computational Multiphase Flows. 9. 26-31.

X Garcia, D Pavlidis, GJ Gorman, JLMA Gomes, MD Piggott, E Aristodemou, J Mindel, JP Latham, CC Pain, H ApSimon, 2011. A two-phase adaptive finite element method for solid-fluid coupling in complex geometries. International Journal for Numerical Methods in Fluids. 66. 82-96. DOI: 10.1002/fld.2249

W Ham, A Vijayan, N Schulte, JD Herner, 2017. Commuter exposure to PM2.5, BC, and UFP in six common transport microenvironments in Sacramento, California. Atmospheric Environment. 167. 335-345.

S Hankey, JD Marshall, 2015. On-bicycle exposure to particulate air pollution: Particle number, black carbon, PM2.5, and particle size. Atmospheric Environment. 122. 65-73.

M Irwin, H Bradley, M Duckhouse, M Hammond, MS Peckham, 2018. High spatio-temporal resolution pollutant measurements of on-board vehicle emissions using ultra-fast response gas analyzers. Atmospheric Measurement Techniques. 11. 3559-3567. https://doi.org/10.5194/amt-11-3559-2018

L Int Panis, S Broekx, R Liu, 2006. Modelling instantaneous traffic emission and the influence of traffic speed limits. Science of the Total Environment. 371. 270-285.

L Int Panis, B de Geus, G Vandenbulcke, H Willems, B Degraeuwe, N Bleux, V Mishra, I Thomas, R Meeusen, 2010. Exposure to particulate matter in traffic: A comparison of cyclists and car passengers. Atmospheric Environment. 44. 2264-2270.

N Jarrin, S Benhamadouche, D Laurence, R Prosser, 2006. A synthetic-eddy-method for generating inflow conditions for large-eddy simulations. International Journal of Heat and Fluid Flow. 27. 585-593.

P Kastner-Klein, E Fedorovich, MW Rotach, 2001. A wind tunnel study of organized and turbulent air motions in urban street canyons. Journal of Wind Engineering and Industrial Aerodynamics. 89. 849-861.

P Kastner-Klein, E Fedorovich, M Ketzel, R Berkowicz, R Britter, 2003. The Modelling of Turbulence from Traffic in Urban Dispersion Models – Part II: Evaluation Against Laboratory and Full-Scale Concentration Measurements in Street Canyons. Environmental Fluid Mechanics. 3. 145-172.

Y Kim, L Huang, S Gong, CQ Jia, 2016. A new approach to quantifying vehicle induced turbulence for complex traffic scenarios. Chinese Journal of Chemical Engineering. 24 (1). 71-78.

S Kingham, I Longley, J Salmond, W Pattinson, K Shrestha, 2013. Variations in exposure to traffic pollution while travelling by different modes in a low density, less congested city. Environmental Pollution. 181. 211-218.

R O'Driscoll, HM ApSimon, T Oxley, N Molden, MEJ Stettler, A Thiyagarajah, 2016. A Portable Emissions Measurement System (PEMS) study of NOx and primary NO2 emissions from Euro 6 diesel passenger cars and comparison with COPERT emission factors. Atmospheric Environment. 145. 81-91.

CC Pain, AP Umpleby, CRE de Oliveira, AJH Goddard, 2001. Tetrahedral mesh optimization and adaptivity for steady-state and transient finite element calculations. Computer methods in applied mechanics and engineering. 190. 3771-3796.

D Pavlidis, GJ Gorman, JLMA Gomes, CC Pain, H ApSimon, 2010. Synthetic-Eddy Method for Urban Atmospheric Flow Modelling. Boundary-Layer Meteorology. 136 (2). 285-299.

W Pearce, CJ Baker, 1997. Wind-tunnel investigation of the effect of vehicle motion on dispersion in urban canyons. Journal of Wind Engineering and Industrial Aerodynamics. 69-71. 915-926.

PTV Group. PTV Vissim. [Online]. Retrieved from http://vision-traffic.ptvgroup.com/en-us/products/ptv-vissim

Y Qin, 1993. Dispersion of vehicular emission in street canyons, Gaungzhou City, South China (P.R.C.). Atmospheric Environment. 27B (3). 283-291.

MS Ragettli, E Corradi, C Braun-Fahrländer, C Schindler, A de Nazelle, M Jerrett, RE Ducret-Stich, N Künzli, HC Phuleria, 2013. Commuter exposure to ultrafine particles in different urban locations, transportation modes and routes. Atmospheric Environment. 77. 376-384.

I Rivas , P Kumar, A Hagen-Zanker, M de Fatima Andrade, AD Slovic, JP Pritchard, KT Geurs, 2017. Determinants of black carbon, particle mass and number concentrations in London transport microenvironments. 161. 247-262.

E Solazzo, X Cai, S Vardoulakis, 2008. Modelling wind flow and vehicle-induced turbulence in urban streets. Atmospheric Environment. 42. 4918-4931.

M Tientcheu-Nsiewe, D Tcheukam-Toko, F Murzyn, A Mehel, B Patte-Rouland, 2016. Numerical Study of a Turbulent Flow in the Near-Wake of an Ahmed Body. American Journal of Environmental Engineering. 6(6). 157-163.

P Thaker, S Gokhale, 2016. The impact of traffic-flow patterns on air quality in urban street canyons. Environmental Pollution. 208. 161-169.

F Yang, Daya Kaul, K Chun Wong, D Westerdahl, L Sun, Kin-fai Ho, L Tian, P Brimblecombe, Z Ning, 2015. Heterogeneity of passenger exposure to air pollutants in public transport microenvironments. 109. 42-51.

Y Zhang, Z Gu, C Wah Yu, 2017. Large eddy simulation of vehicle induced turbulence in an urban street canyon with a new dynamically vehicle-tracking scheme. Aerosol and Air Quality Research. 17. 865-874.